Electrical Power and Energy Systems 84 (2017) 153–167

Contents lists available at ScienceDirect

Electrical Power and Energy Systems

journal homepage: www.elsevier.com/locate/ijepes

Power quality enhancement using fuzzy sliding mode based pulse width modulation control strategy for unified power quality conditioner

Rajesh Kumar Patjoshi *, Venkata Ratnam Kolluru, Kamalakanta Mahapatra

Electronics and Communication Engg. Dept., National Institute of Technology Rourkela, India

ARTICLE INFO

Article history:
Received 4 January 2016
Received in revised form 3 March 2016
Accepted 13 May 2016

Keywords:
FSMPWM
Power quality
Sliding surface
Mamdani based fuzzy
Chattering effects
Fixed switching

ABSTRACT

This paper proposes a fixed switching methodology based on fuzzy sliding mode pulse width modulation (FSMPWM) control strategy for three-phase three-wire unified power quality conditioner (UPQC). The proposed FSMPWM control technique eliminates numerous power quality (PQ) problems such as current harmonics, load unbalance, voltage sag/swell, voltage unbalance, voltage distortion and phase-angle jump existing in the power distribution network. Initially, the design of FSMPWM is based on the implementation of sliding surface by proper extraction of reference current and voltage signals for UPQC. Subsequently, the equivalent control law is formulated for both shunt and series converter. With this consideration, Mamdani fuzzy rule base is designed at the sliding surface for generation of switching pulse. Moreover, the proposed method eliminates the chattering effects by smoothing the control law in a narrow boundary layer for generating fixed switching pulse for both shunt and series converter. The performance of proposed UPQC system has been simulated and analyzed by MATLAB/SIMULINK followed by real-time experimental studies accomplished with a real-time-hardware-in the loop (HIL) system in OPAL-RT simulator. Additionally, the efficacy of this proposed technique is compared with a conventional sliding mode controller (CSMC).

Introduction

UPQC is a custom power device (CPD) utilized for eliminating the PQ problems such as harmonics [1] unbalance, sag and swell and phase-angle jump due to the extensive usage of electronically switched devices and non-linear load [2,3]. This CPD comprises of both shunt and series converters coupled through a common DC-link voltage and deals with harmonics in load current and also imperfections in source voltage [4]. The shunt converter can eliminate current harmonics and unbalances from the nonlinear load so that perfect sinusoidal current flows through the power network, however series converter can compensate voltage sag/swell, voltage unbalance, voltage distortion and phase-angle jump present on the source side, so that perfect voltage regulation is maintained across the load [5].

Therefore, UPQC draws the consideration of power engineers to create active and adaptable solutions to PQ issues, which leads to the development of novel topologies and advanced control systems for UPQC. Control system plays an important part in the overall performance of a power conditioner. The quick detection of disturbance signal and fast extraction of reference signal are the main requirements for perfect compensation. Some advanced control techniques have been reported for UPQC in the literature, which include neural networks, SRF and PSO based controller [6–8]. However, these controllers are mainly used for reference signal generation and not so much useful in generation of pulse width modulation (PWM) signal. PWM controllers such as Hysteresis, triangular carrier and space vector modulation (SVM) [9–11] are failed to track the reference signal properly during load and supply side perturbations, therefore compensation capability of UPQC is degraded.

Recently, many control techniques like deadbeat control, repetitive controller and Fuzzy PWM controller [12–14] have been investigated to accomplish the aforementioned demands. Additionally, harmonics elimination method and nonlinear observer strategy are employed to improve the transient response. However, these control techniques utilize average modeling technique of the converter [15]. As the state space equations of converter vary with switching states, power converters suffer from discontinuous control [16]. The inherent switching nature of power converters is compatible with sliding mode controller (SMC) [17,18]. Moreover, the SMC is popular for its stability, robustness, good regulation and frequent switching action under all operating conditions of load and supply voltage.

* Corresponding author.
E-mail address: rajeshpatjoshi1@gmail.com (R.K. Patjoshi).

http://dx.doi.org/10.1016/j.ijepes.2016.05.007
0142-0615/

Irrespective of excellent performance, SMC suffers from chattering problem, which leads to generate a variable switching frequency causing switching and power losses, as well as electromagnetic compatibility (EMC) noise. To avoid this drawback, a fuzzy logic controller is considered in conjunction with SMC to generate a fixed switching methodology. This Fuzzy-logic SMC [19–21] is one of the promising solutions to handle power systems uncertainty, as well as nonlinearity situations. Power system uncertainty arises due to random variation of system loads, irregular fluctuations of system parameter such as capacity of distribution line and sudden failure of system component of the power line. To operate UPQC in the above uncertainty conditions, a fuzzy SMC based PWM technique is proposed for accurately tracking the reference signal, which provides better compensation capability of UPQC.

The objective of this study is to improve the power quality in power distribution network by employing novel FSMPWM technique. This control method generates a fixed switching PWM signal, which reduces the excessive power losses and EMC noise generated by UPQC and also simplifies the series LC filter design. As a consequence, it is efficient in elimination of PQ issues such as current harmonics, load unbalance, voltage distortion, voltage sag/swell, voltage unbalance and phase-angle jump present in the power distribution network. The proposed FSMPWM based control scheme considers s, $\dot{s}$ as input fuzzy variables and the fuzzy rule base table is constructed by using two-dimensional spaces. This table will have 49 rules with s and $\dot{s}$ having seven triangular membership functions each. A singleton output membership function is used for the defuzzification purpose for generating switching pulse for both shunt and series converters. Moreover, reduction of mathematical operands, insensitiveness to the system uncertainty and external disturbance are the main advantages of this proposed method, which facilitates a simpler hardware control circuit. The performance of the proposed control strategy was simulated, analyzed and investigated using MATLAB/SIMULINK followed by real-time experimental studies accomplished by using hardware-in-loop (HIL) system in OPAL-RT simulator and also a comparative study has been pursued employing CSMC [22] and the proposed one.

UPQC power circuit configuration

The power circuit configuration of UPQC is shown in Fig. 1. It comprises of series converter and shunt converter. The series converter is a three phase PWM voltage source inverter, which mitigates voltage sag, swell, voltage distortion and voltage unbalance existing in the supply voltage. Subsequently, the *LC* filter consists of inductor L_{sef} and capacitor C_{ef} connected in output of series converter to prevent the flow of switching ripples. Similarly, the transformers are connected at the output of the *LC* filter to provide isolation between series converter and the power line and also prevent the DC-link capacitor from being short circuited due to the operation of various switches. The power circuit of shunt converter consists of a three phase PWM voltage source inverter, which is connected through an interfacing inductor L_{shf} to provide isolation between the shunt converter and power line. The purpose of shunt converter is to restrain the load current harmonics and to control the DC-link voltage. However, insulated gate bipolar transistors (IGBTs) with anti-parallel diodes are used as PWM voltage source inverter and a 3-phase diode-bridge rectifier employed with resistive R_L as well as inductive L_L are used as a nonlinear load.

Reference current generation for shunt converter

The proposed control strategy shown in Fig. 2 is employed to generate a reference current signal as well as PWM signal for shunt converter of UPQC. At first reference current signal is generated by considering the peak amplitude of source current $I_{\max}$ generated from the PI-controller (Proportional constants: $k_p = 0.2475$ and Integral constant: $k_i = 8.7500$). This peak value of the reference current is produced by regulating DC-link capacitor voltage V_{dc} of UPQC [23]. Commonly, a PI-controller is utilized for determining the magnitude of this $I_{\max}$ from the error between the average voltage across the DC-link capacitor V_{dc} and the reference voltage V^*_{dc}. Thus, reference source currents described in Eq. (1) are generated by multiplying $I_{\max}$ with the unit vector (U_{sa}, U_{sb}, U_{sc}) signal generated from the phase locked loop (PLL) [24] block that is shown in Fig. 3.

$$\begin{aligned} I^*_{Sa} &= I_{\max} \times U_{sa} \\ I^*_{Sb} &= I_{\max} \times U_{sb} \\ I^*_{Sc} &= I_{\max} \times U_{sc} \end{aligned} \tag{1}$$

Fuzzy sliding mode control of shunt converter

To apply the fuzzy sliding mode control (FSMC) theory to the shunt converter, sliding surfaces are developed and based on which equivalent control laws are designed. Then, PWM signals are generated by utilizing Mamdani based fuzzy system at the sliding surface.

For designing sliding surface, the equivalent circuit for one leg of shunt converter is considered, which is illustrated in Fig. 4. Sliding mode control law depending upon switching function 'u' is considered here. When either S1 or D1 conducts, then $u = 1$, and when either S2 or D2 conducts, then $u = -1$. The inductor current is given by the following expression,

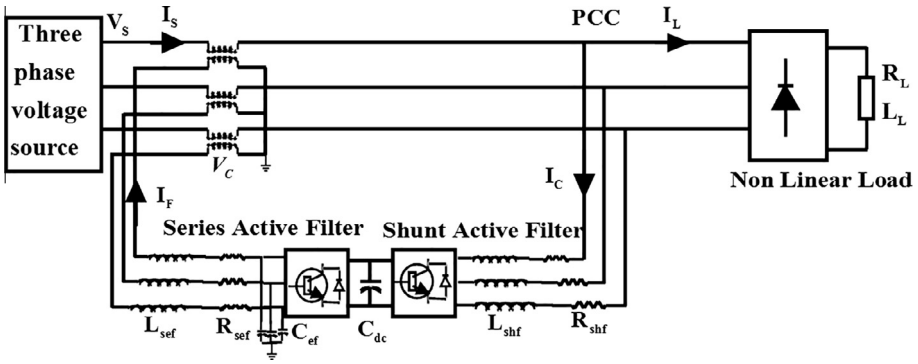

Fig. 1. Power circuit configuration for UPQC.

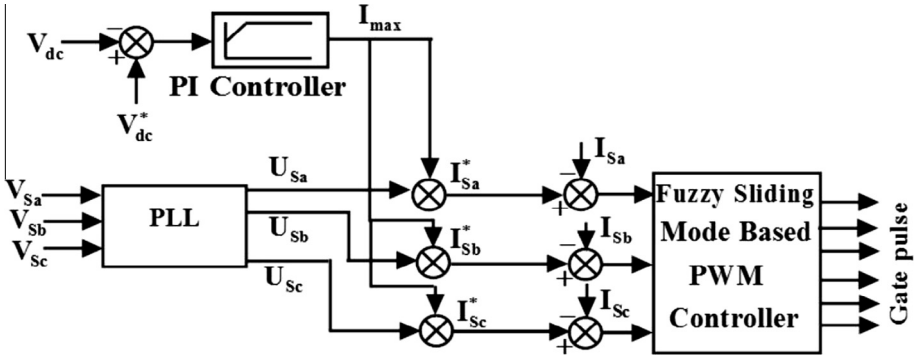

Fig. 2. Control structure of shunt converter using the proposed FSMC scheme.

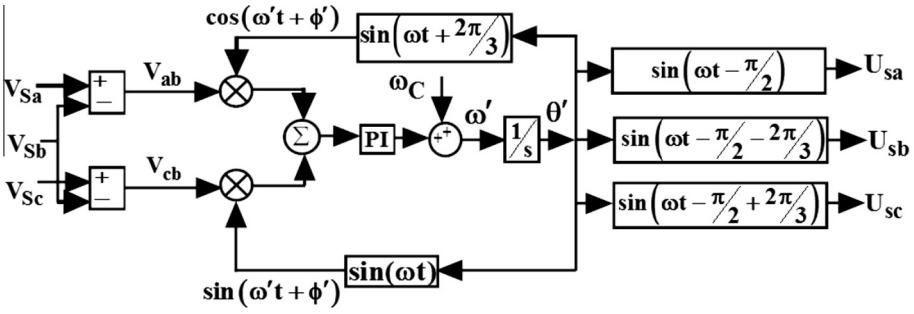

Fig. 3. PLL circuit block diagram.

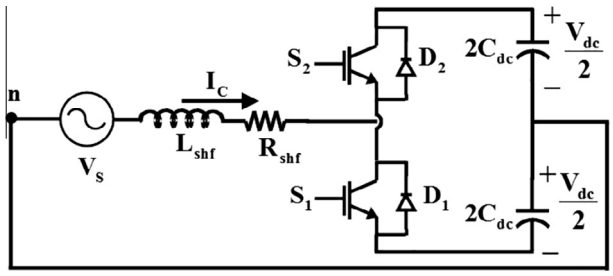

Fig. 4. Equivalent circuit for one leg of the shunt converter.

$$\frac{dI_C}{dt} = \frac{V_S}{L_{shf}} - u\frac{V_{dc}}{2L_{shf}} - \frac{R_{shf}}{L_{shf}}I_C \tag{2}$$

The capacitor voltage equation considering the ripple due to compensating currents can be expressed as

$$\frac{dV_{dc}}{dt} = -\frac{1}{2}\left[u_a\frac{I_{Ca}}{C_{dc}} + u_b\frac{I_{Cb}}{C_{dc}} + u_c\frac{I_{Cc}}{C_{dc}}\right] \tag{3}$$

where u_a, u_b and u_c are the switching functions along with I_{Ca}, I_{Cb} and I_{Cc} are the filtering currents for three phases a, b and c respectively. Applying KCL at point of common coupling (PCC), the following current equation can be obtained.

$$I_{Sx} = I_{Lx} + I_{Cx} = I_{Lx} + \int\left[\frac{V_{Sx}}{L_{shf}} - u_x\frac{V_{dc}}{2L_{shf}} - \frac{R_{shf}}{L_{shf}}I_{Cx}\right]dt \tag{4}$$

where 'x' denotes the phase sequence of three phase signal.

The fuzzy sliding surface trajectory is achieved by deducting the measured source current I_{Sx} from the reference source current I^*_{Sx}. An usual form of sliding surface for shunt converter is given by

$$s(t) = e_x(t) \tag{5}$$

where

$$e_x(t) = [I^*_{Sx} - I_{Sx}] = 0 \tag{6}$$

For the shunt converter, the expression for $\dot{s}(t)$ can be written as

$$\dot{s}(t) = \dot{e}_x(t) \tag{7}$$

Thus, $\dot{e}_x(t) = (\dot{I}^*_{Sx} - \dot{I}_{Sx})$

Applying the value of $\dot{I}_{Cx}$ in Eq. (8), the value of $\dot{e}_x(t)$ becomes

$$= \left(\frac{dI^*_{Sx}}{dt} - \left(\frac{dI_{Cx}}{dt} + \frac{dI_{Lx}}{dt}\right)\right) = \left(\frac{dI^*_{Sx}}{dt} - \frac{V_{Sx}}{L_{shf}} + \frac{R_{shf}}{L_{shf}}I_{Cx} + u_x\frac{V_{dc}}{2L_{shf}} - \frac{dI_{Lx}}{dt}\right) \tag{8}$$

By setting the sliding surface $\dot{e}_x(t) = 0$ the equivalent control law can be defined as

$$u_{eqx} = \left(\frac{dI_{Lx}}{dt} + \frac{V_{Sx}}{L_{shf}} - \frac{dI^*_{Sx}}{dt} - \frac{R_{shf}}{L_{shf}}I_{Cx}\right)\left(\frac{2L_{shf}}{V_{dc}}\right) \tag{9}$$

The natural control limits of the circuit are $-1 \leqslant u_{eqx} \leqslant 1$; this expression could be utilized for establishing the design procedure and performance of the shunt converter. It can be seen that Eq. (8) is linear with respect to u_x such that

$$\begin{aligned} &\text{If } u_x < u_{eqx} \text{ then } \dot{e}_x < 0 \\ &\text{If } u_x > u_{eqx} \text{ then } \dot{e}_x > 0 \end{aligned} \tag{10}$$

where u_x is the actual control signal of shunt converter.

Further the equivalent control is driven by the natural bounds of the circuit i.e., $-1 \leqslant u_{eqx} \leqslant 1$, from which the following expressions can be summarized.

$$\begin{aligned} &\text{If } u_x = 1 \text{ then } \dot{e}_x < 0 \\ &\text{If } u_x = -1 \text{ then } \dot{e}_x > 0 \end{aligned} \tag{11}$$

To satisfy $e_x\dot{e}_x \leqslant 0$, the discontinuous control law can be seen by applying the variable e_x and $\dot{e}_x$ to the fuzzy controller and fuzzy controller must be satisfying the condition of Eq. (12) for generating the PWM signal for shunt converter.

$$u_x(t) = \begin{cases} 1 \text{ for } s(e_x,t) < 0 \\ 0 \text{ for } s(e_x,t) = 0 \\ -1 \text{ for } s(e_x,t) > 0 \end{cases} \quad (12)$$

The block diagram of proposed FSMPWM controller for shunt converter is displayed in Fig. 5(a). Here e_x and $\dot{e}_x$ are the inputs and $u(t)$ represents the output of the FSMPWM. Further, $e_x(t)$ and $\dot{e}_x(t)$ are the fuzzified variables and $u_x(t)$ is the defuzzified output in the form of switching pulse. Universe of discourse of $e_x(t)$ and $\dot{e}_x(t)$ are arranged from −25 to 25 whereas output universe of discourse are arranged from −1 to 1, thus the range of nonfuzzy variables e_x and $\dot{e}_x$ must be scaled by suitable gains $k1$ and $k2$ to fit the universe of discourse of fuzzified variables $e_x(t)$ and $\dot{e}_x(t)$. In this case $\dot{e}_x(t)$ is approximated with $(e(t)_k - e(t)_{k-1})/T$, where T is the sampling period. Here we choose triangular type membership functions for the fuzzification of the input variable and singleton membership function as a defuzzified output variable, as shown in Figs. 5(b) and 6. The FSMPWM has to use the natural control conditions called Lyapunov stability conditions $e_x(t)\dot{e}_x(t) < 0$ with consideration of $e_x(t)$ and $\dot{e}_x(t)$ be the fuzzy variables of the system.

The rule table shown in Table 1 is constructed by using two dimensional space i.e., $e_x(t)$ and $\dot{e}_x(t)$, each having seven triangular membership functions with 49 fuzzy rules. Now, we choose a Lyapunov function for stability analysis,

$$V(t) = \frac{1}{2} e_x(t)^2 \quad (13)$$

Then

$$\dot{V}(t) = e_x(t)\dot{e}_x(t) \quad (14)$$

Based on qualitative analysis described in above and the Lyapunov stability condition ($e_x(t) = 0$ and $\dot{V}(t) < 0$), the sliding surface is asymptotically stable and simultaneously matches the reaching conditions $e_x(t)\dot{e}_x(t) < 0$.

The Mamdani's min-operation fuzzy inference system and the singleton defuzzification method for generating switching pulse for shunt converter are considered here. The control rules of Table 1 are defined below:

(1) If $e_x(t)$ is PB and $\dot{e}_x(t)$ is PB, then $u_x(t)$ is NB.

This control rule implies that if $e_x(t)$ and $\dot{e}_x(t)$ are both positive big ($e_x(t)\dot{e}_x(t)$ is largely positive), then a large negative change in the control input is required to decrease $e_x(t)\dot{e}_x(t)$ quickly.

(2) If $e_x(t)$ is PB and $\dot{e}_x(t)$ is NB, then $u_x(t)$ is ZE.

This control rule implies a situation where $e_x(t)$ is positive big and $\dot{e}_x(t)$ is negative big (no changes in $e_x(t)\dot{e}_x(t)$), then there is no change in the control input.

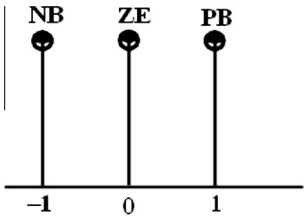

Fig. 6. Membership functions for the output variable.

Table 1
Rule based table for shunt FSMC.

$e_x/\Delta e_x$	NB	NM	NS	ZE	PS	PM	PB
NB	PB	PB	PB	ZE	NB	NB	NB
NM	PB	PB	PB	ZE	NB	NB	NB
NS	PB	PB	PB	ZE	NB	NB	NB
ZE	PB	PB	PB	ZE	NB	NB	NB
PS	PB	PB	ZE	ZE	NB	NB	NB
PM	PB	ZE	ZE	NB	NB	NB	NB
PB	ZE	ZE	ZE	NB	NB	NB	NB

Reference voltage generation for series converter

Fig. 7 shows the control structure for generating a reference voltage signal as well as fixed frequency PWM signal for series converter of UPQC. Initially, the proposed control strategy is employed to create reference compensating voltage for defining sliding surface. For achieving this goal, the following desired three-phase load voltages specified in Eq. (15) are multiplied with the source currents in Eq. (16) for generating the required power.

$$\begin{aligned} V_{La} &= V_m \sin(\omega_1 t + \varphi) \\ V_{Lb} &= V_m \sin(\omega_1 t - 120^\circ + \varphi) \\ V_{Lc} &= V_m \sin(\omega_1 t + 120^\circ + \varphi) \end{aligned} \quad (15)$$

$$\begin{aligned} I_{Sa} &= I_m \sin(\omega_1 t + \varphi) \\ I_{Sb} &= I_m \sin(\omega_1 t - 120^\circ + \varphi) \\ I_{Sc} &= I_m \sin(\omega_1 t + 120^\circ + \varphi) \end{aligned} \quad (16)$$

where V_m, I_m and φ are the magnitude of supply voltage, current and phase angle respectively. Based on the condition of load active power delivered from the supply, it is necessary to determine the reference load voltage from magnitude V_{max} from the source current peak detector and instantaneous load current and load voltage components. The three-phase instantaneous (rms) load current can be signified as

$$I_{Lx} = \sum_{n=1}^{\infty} I_{xn}^{+} + \sum_{n=1}^{\infty} I_{xn}^{-} + \sum_{n=1}^{\infty} I_{xn}^{\circ} \quad (17)$$

where x denotes the phase sequence and 0, +, − represent the zero, positive and negative-sequence components respectively and n

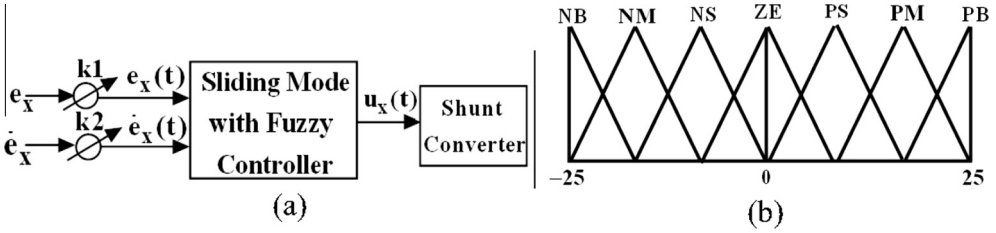

Fig. 5. FSMC for shunt converter, (a) block diagram representation and (b) membership functions for the input variable $e_x(t)$ and $\dot{e}_x(t)$.

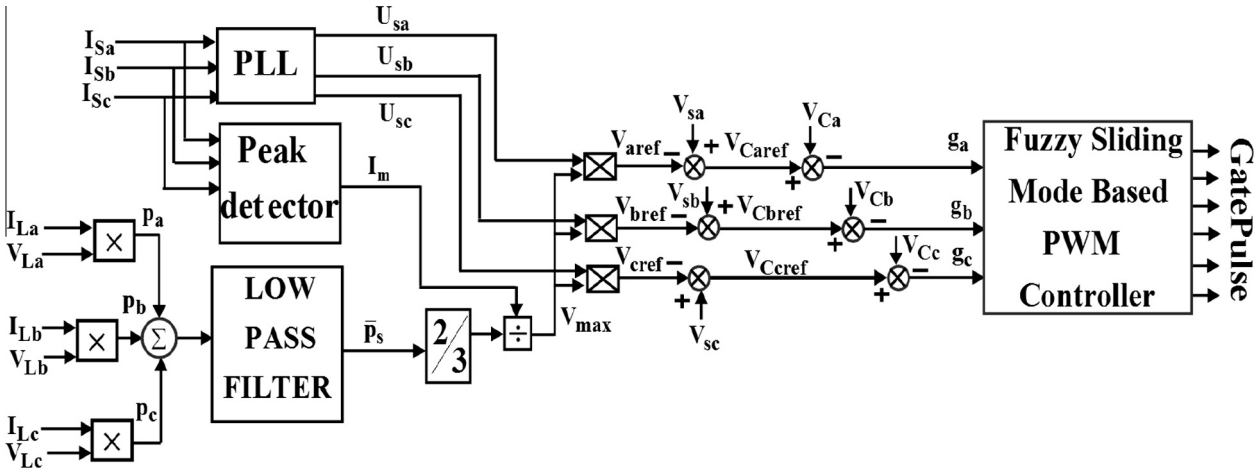

Fig. 7. Control structure of series converter using the proposed FSMC scheme.

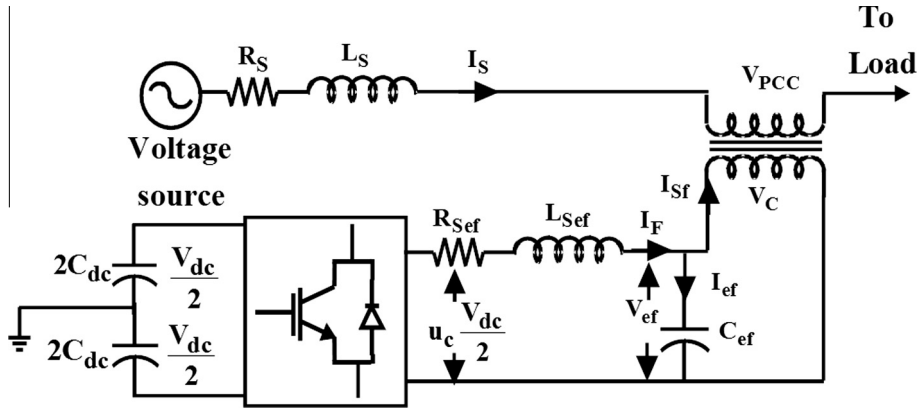

Fig. 8. Equivalent circuit for a single phase series converter.

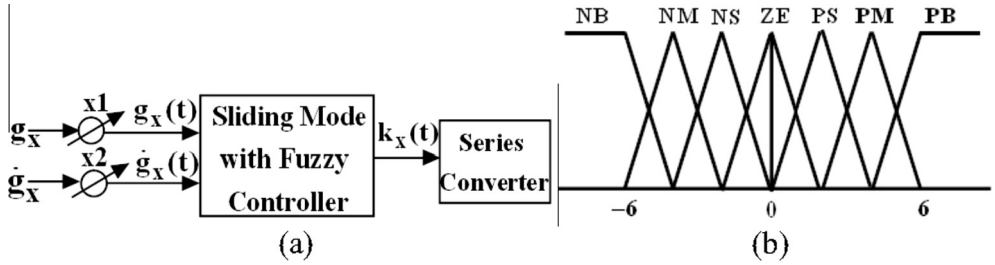

Fig. 9. FSMC for series converter, (a) block diagram representation and (b) membership functions for the input variable $\dot{g}(t)$ and $\ddot{g}(t)$.

Table 2
Rule based table for series FSMC.

$\dot{g}/\Delta\dot{g}$	NB	NM	NS	ZE	PS	PM	PB
NB	NB	NB	NB	ZE	PB	PB	PB
NM	NB	NB	NB	ZE	PB	PB	PB
NS	NB	NB	NB	ZE	PB	PB	PB
ZE	NB	NB	NB	ZE	PB	PB	PB
PS	NB	NB	ZE	ZE	PB	PB	PB
PM	NB	ZE	ZE	PB	PB	PB	PB
PB	ZE	ZE	ZE	PB	PB	PB	PB

signifies the harmonic components number. Hence, positive sequence active power consumed by the load can be represented by

$$p_{l1}^{+} = \frac{1}{T}\int_0^T \sum_{x\in k} V_{Lx} I_{Lx} dt = \frac{3V_{\max} I_m}{2} \tag{18}$$

Table 3
Simulation parameter.

$V_{rms} = 360$ V	$V_{dc}^{*} = 620$ V	$R_L = 20\ \Omega$	$R_S = 0.1\ \Omega$
$L_L = 22$ mH	$L_S = 0.1$ mH	$C_{dc} = 4000$ μf	$R_{sef} = 0.2\ \Omega$
$R_{shf} = 0.5\ \Omega$	$L_{sef} = 8$ mH	$L_{shf} = 2.5$ mH	$C_{ef} = 2$ μf

where $p_{l1}^{+} = p_{s1}^{+}$.

However, p_{l1}^{+} denotes the positive sequence active power consumed by the load and p_{s1}^{+} is the positive sequence active power delivered by the supply. The output of the low pass filter p_{l1}^{+} and the peak amplitude of source current I_m are utilized for generating the peak amplitude of load voltage $V_{\max}$ as described in Eq. (19),

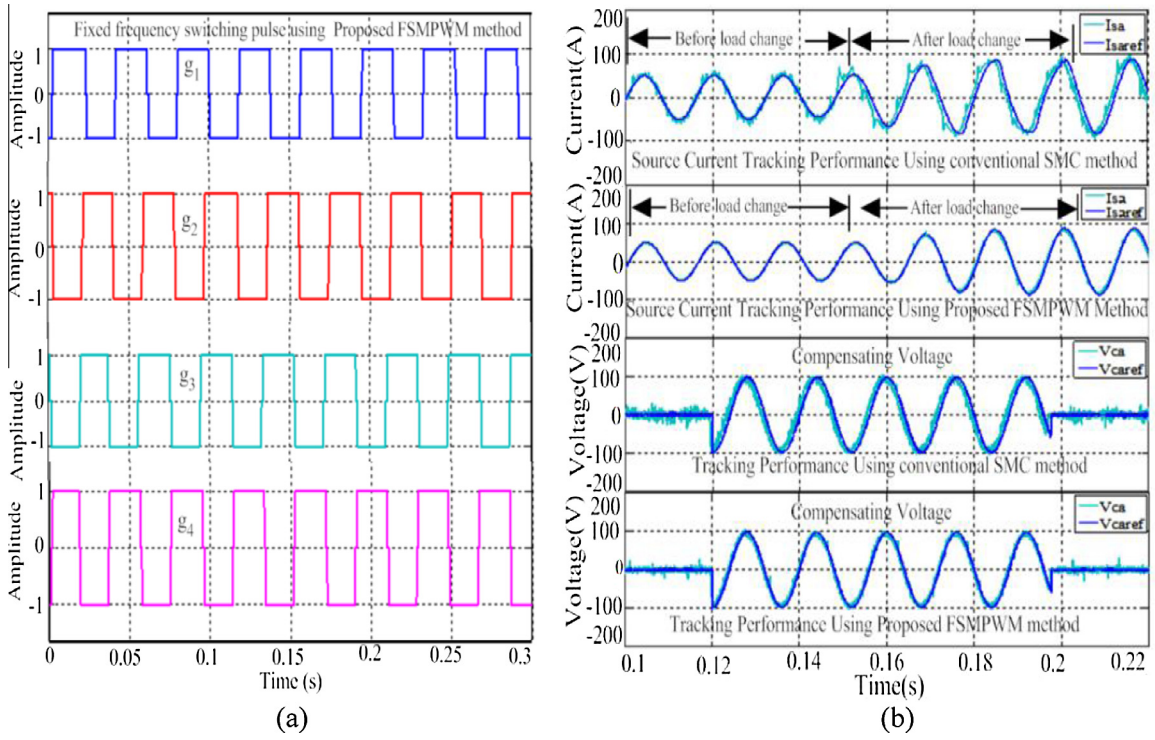

Fig. 10. Switching pulse and tracking performance of proposed algorithm (a) fixed frequency switching pulse using proposed FSMPWM method and (b) tracking performance comparison of proposed FSMPWM and conventional SMC method.

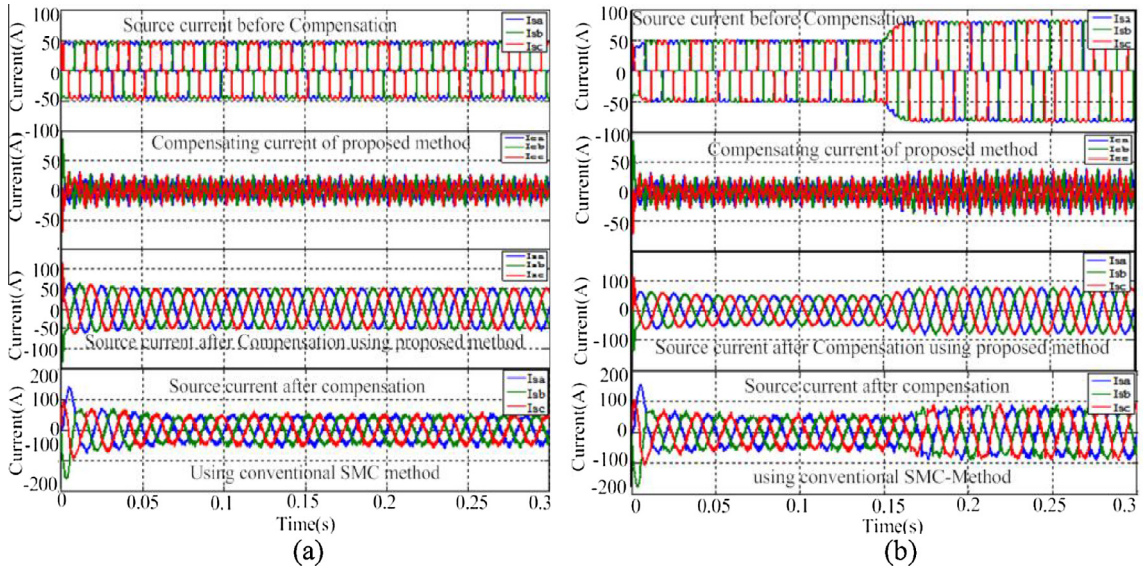

Fig. 11. Simulation result of shunt converter, (a) shunt converter compensation waveforms during steady state condition and (b) shunt converter compensation waveforms during transient state condition.

then the reference voltage V_{xref} is found by multiplying unit sine vector U_{Sx} and $V_{\max}$ as described in Eq. (20).

$$V_{\max} = \frac{2p_{l1}^{+}}{3I_m} = \frac{2\bar{p}_s}{3I_m} \tag{19}$$

$$V_{xref} = V_{\max} * U_{Sx} \tag{20}$$

The compensating reference voltage V_{Cxref} for trajectories of sliding surface is found by subtracting the reference source voltage V_{xref} from supply voltage V_{Sx} as given in Eq. (21).

$$V_{Cxref} = V_{Sx} - V_{xref} \tag{21}$$

Fuzzy sliding mode control of series converter

Fig. 8 shows the single phase equivalent circuit of series converter for the analysis of FSMC. The voltage and current at the converter side are represented as $u_c \frac{V_{dc}}{2}$ and I_F respectively. The ac-filter capacitor voltage and current are signified as V_{ef} and I_{ef} respectively. The voltage and current at the grid side are represented as

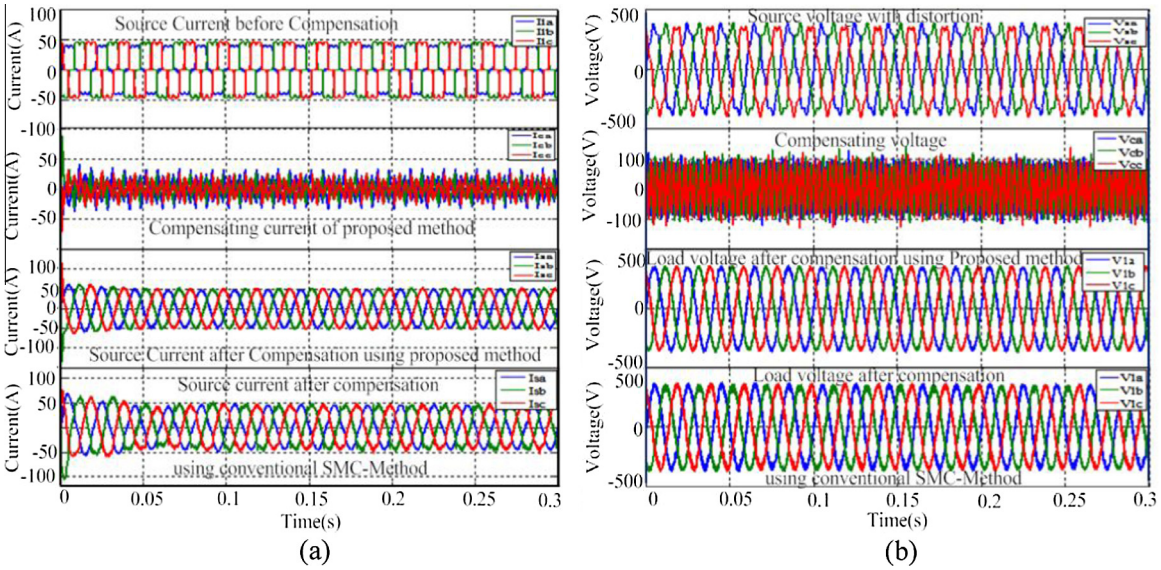

Fig. 12. Simulation result of shunt and series converter (a) shunt converter compensation waveform during load unbalance condition and (b) series converter compensation waveform during voltage distortion condition.

Table 4
THD comparison of proposed and SMC control method.

Control method	THD before compensation				THD after compensation			
	Source current			Load voltage under distortion condition (%)	Source current			Load voltage After compensation (%)
	Steady-state condition (%)	Transient-state condition (%)	Load-unbalance condition (%)		Steady-state condition (%)	Transient-state condition (%)	Load-unbalance condition (%)	
CSMC [22]	31.25	33.42	30.61	10.24	3.43	4.37	3.36	2.86
FSMPWM	31.25	33.42	30.61	10.24	2.16	2.36	2.12	1.52

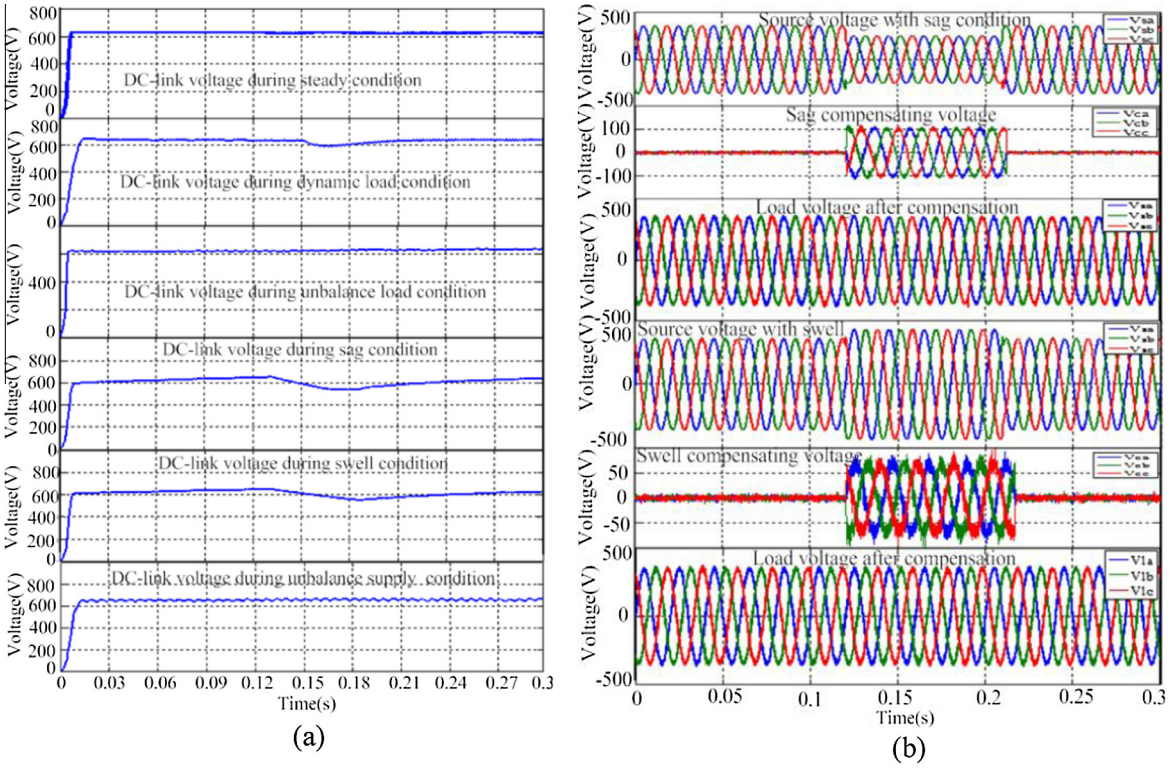

Fig. 13. Simulation result of DC-link voltage and sag/swell compensation, (a) DC-link voltage waveforms of shunt and series converter and (b) sag and swell compensation waveforms with the proposed method.

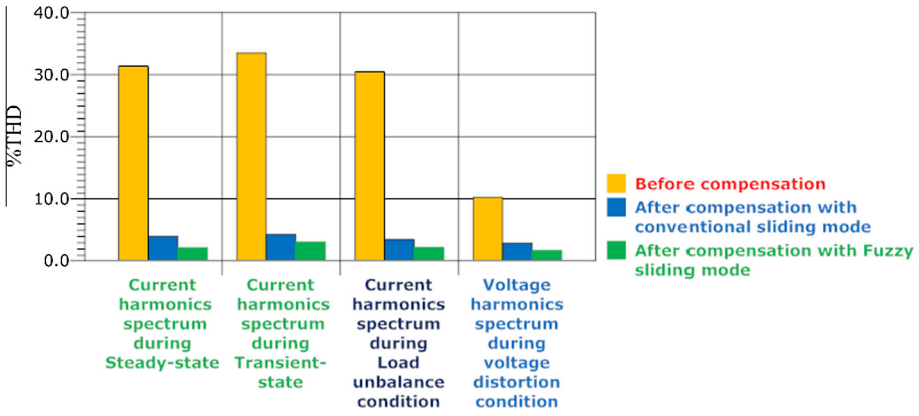

Fig. 14. Current and voltage THD results for proposed and conventional SMC method.

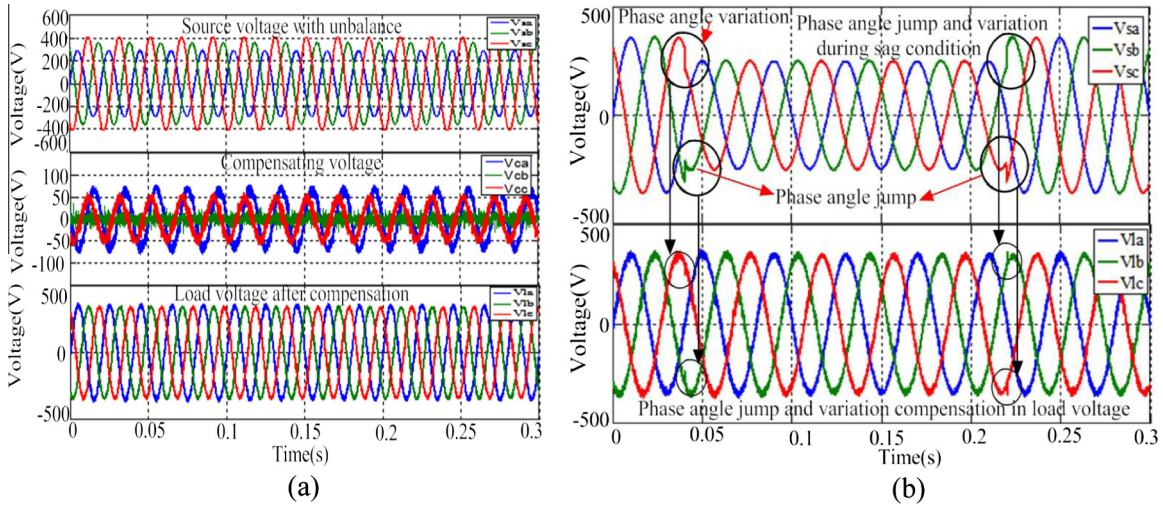

Fig. 15. Simulation result of unbalance supply voltage and phase-angle jump, (a) supply voltage unbalance compensation waveform with the proposed method and (b) phase-angle jump and variation compensation during sag condition.

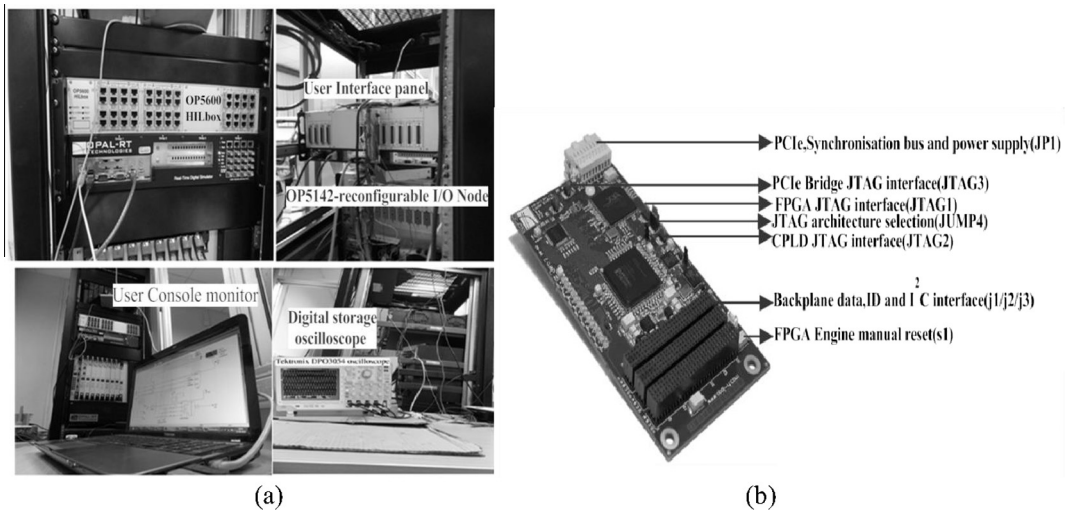

Fig. 16. Laboratory Experimental setup, (a) real time HIL system and (b) OP5142 connectors and layout.

V_C and I_{sf} respectively. The essential assumption would be that, the injected voltage is equivalent to the voltage across the filter capacitor ($V_{ef} = V_C$) of the series converter and the injection transformer is recognized as ideal with 1: n turn ratio. With these assumptions, voltage and current at the output terminal of the series converter can be written as

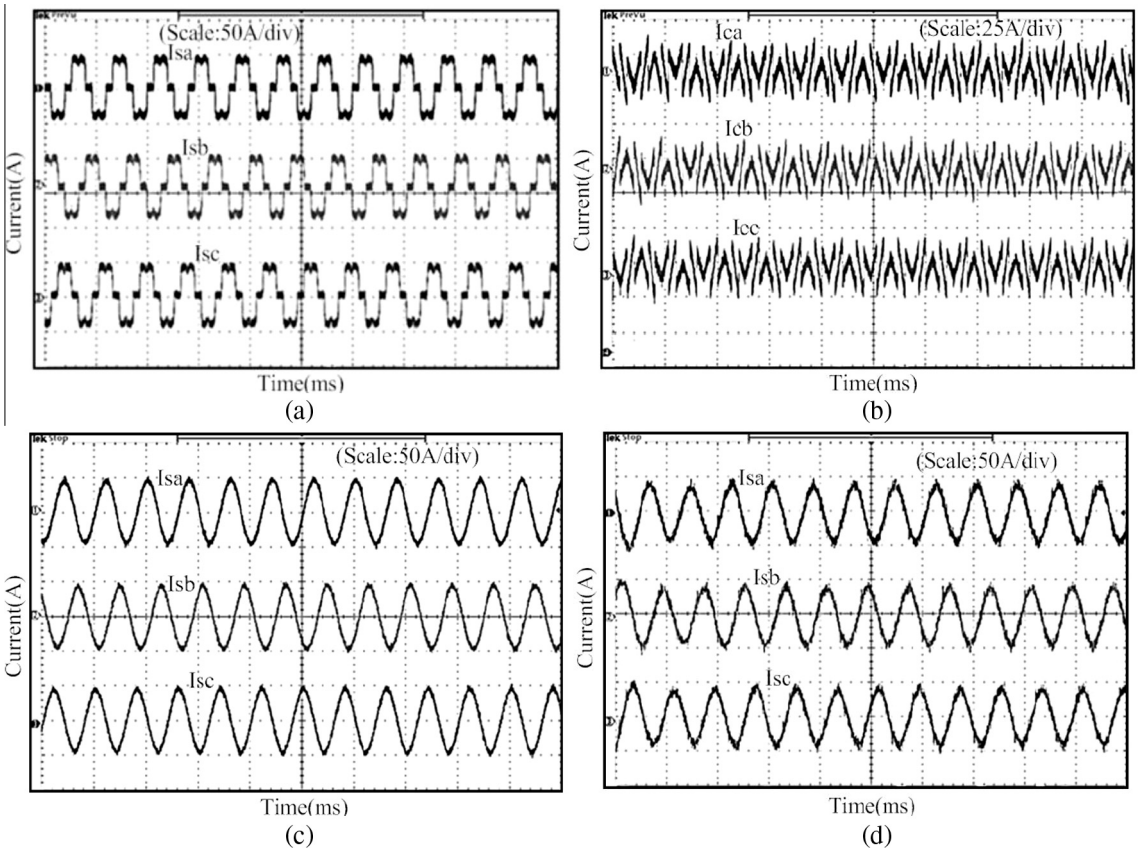

Fig. 17. Experimental results during load balanced condition, (a) source current before compensation under steady-state, (b) compensation current under steady-state, (c) source current after compensation under steady-state conditions using proposed method, and (d) source current after compensation under steady-state conditions using conventional SMC method.

$$\frac{dI_F}{dt} = \frac{V_{dc}}{2L_{sef}}u_c - \frac{R_{sef}}{L_{sef}}I_F - \frac{1}{L_{sef}}V_{ef} \tag{22}$$

$$\frac{dV_{ef}}{dt} = \frac{dV_C}{dt} = \frac{1}{C_{ef}}I_F - \frac{1}{C_{ef}}I_{sf} \tag{23}$$

The trajectory of fuzzy sliding surface for series converter is found by deducting the measured compensating voltage V_{Cx} from the reference compensating voltage V_{Cxref}.

Therefore, standard method for selecting the sliding surface for series converter is

$$s_x(t) = \dot{g}_x \tag{24}$$

where 'x' is phase sequence and corresponding error function $g_x(t)$ is defined as,

$$g_x(t) = (V_{Cxref} - V_{Cx}) \tag{25}$$

For the series converter, the expression for $\dot{s}(t)$ can be written as,

$$\dot{s}(t) = \ddot{g}(t) \tag{26}$$

Thus

$$\dot{s}_x(t) = (\ddot{V}_{Cxref} - \ddot{V}_{Cx}) \tag{27}$$

Applying the value of dV_C/dt in Eq. (27), the value of $\dot{s}_x(t)$ becomes

$$\begin{aligned}\dot{s}_x(t) &= \left(\ddot{V}_{Cxref} - \frac{1}{C_{ef}}\dot{I}_{Fx} + \frac{1}{C_{ef}}\dot{I}_{sfx}\right) \\ &= \frac{1}{C_{ef}}\left(-\frac{V_{dc}}{2L_{sef}}u_{cx} + \frac{R_{sef}}{L_{sef}}I_{Fx} + \frac{1}{L_{sef}}V_{efx}\right) + \frac{1}{C_{ef}}\dot{I}_{sfx} + \ddot{V}_{Cxref}\end{aligned} \tag{28}$$

By setting the sliding surface $\dot{s}(t) = 0$ the equivalent control law can be defined as

$$u_{eqcx} = \left(\frac{2R_{sef}}{V_{dc}}I_{Fx} + \frac{2V_{efx}}{V_{dc}} + \frac{2L_{sef}}{V_{dc}}\dot{I}_{sfx} + \frac{\ddot{V}_{Cxref}}{V_{dc}}2C_{ef}L_{sef}\right) \tag{29}$$

The existence of sliding mode is observed by the condition $s(\dot{g}_x, t) = 0$ after obtaining the sliding surface. Hence, the switching law can be expressed by Eq. (30).

$$s(\dot{g}_x, t)\dot{s}(\ddot{g}_x, t) < 0 \tag{30}$$

Thus, the natural control limits of the series converter are $-1 \leqslant u_{eqsx} \leqslant 1$, this expression is used for the equivalent control for both performance and design procedure of the converter. Correspondingly, it is observed that Eq. (28) is linear with respect to u_c such that

$$\begin{aligned}&\text{If } u_c < u_{eqsx} \text{ then } \dot{s}(\ddot{g}_x, t) > 0 \\ &\text{If } u_c > u_{eqsx} \text{ then } \dot{s}(\ddot{g}_x, t) < 0\end{aligned} \tag{31}$$

where u_c is the actual control signal of series converter.

Thus the equivalent control is constrained by the natural bounds of the converter, such that $-1 \leqslant u_{eqsx} \leqslant 1$, and it is seen that

$$\begin{aligned}&\text{If } u_c = -1 \text{ then } \dot{s}(\ddot{g}_x, t) > 0 \\ &\text{If } u_c = 1 \text{ then } \dot{s}(\ddot{g}_x, t) < 0\end{aligned} \tag{32}$$

For fulfillment of above discontinuous control law, the actual error functions $\dot{g}$ and $\ddot{g}$ need to be scaled to their corresponding universe of discourse $\dot{g}(t)$ and $\ddot{g}(t)$ applied to the fuzzy controller as shown in Fig. 9(a). The scaling factors x_1 and x_2 corresponding to $\dot{g}(t)$ and $\ddot{g}(t)$ are arranged from -6 to 6. The output of fuzzy controller is $k(t)$ which is defuzzified output and is arranged from

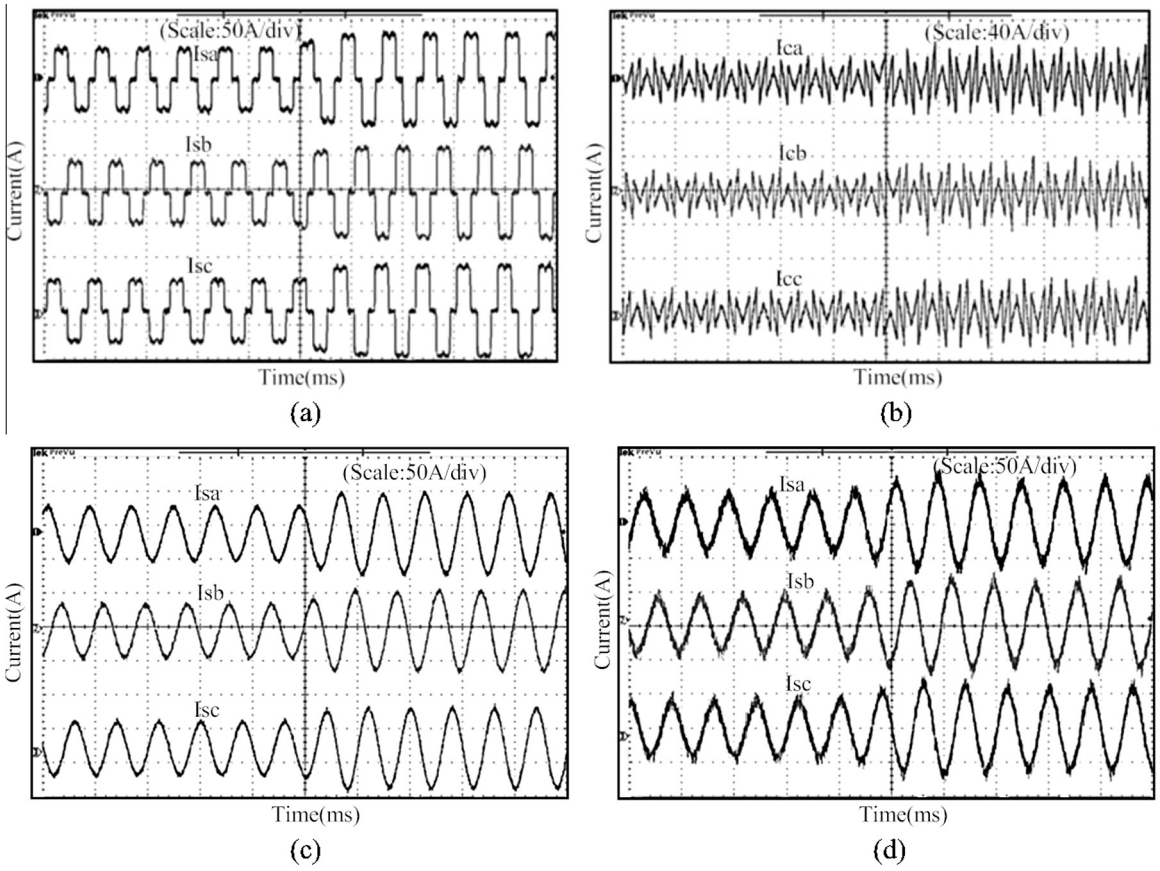

Fig. 18. Experimental results during load transient condition, (a) source current before compensation during transient-state, (b) compensation current during transient-state conditions, (c) source current after compensation during transient-state conditions using proposed method, and (d) source current after compensation during transient-state conditions using conventional SMC method.

−1 to 1. As data manipulation in fuzzy controller is based on the fuzzy set theory, the associated fuzzy subset defined for controlling the series converter are as follows,

$$\dot{g}(t) = \{\text{NB}, \text{NM}, \text{NS}, \text{ZE}, \text{PS}, \text{PM}, \text{PB}\}$$
$$\ddot{g}(t) = \{\text{NB}, \text{NM}, \text{NS}, \text{ZE}, \text{PS}, \text{PM}, \text{PB}\}$$
$$k(t) = \{\text{NB}, \text{ZE}, \text{PB}\}$$

where NB is negative big, NM is negative medium, NS is negative small, ZE is zero, PS is positive small, PM is positive medium and PB is positive big. The membership functions for input fuzzy subsets $\dot{g}(t)$ and $\ddot{g}(t)$ are depicted in Fig. 9(b) and corresponding output membership function $k(t)$ is shown in Fig. 6. The resulting linguistic rule based on FSMC for series active power filter is summed in Table 2. Construction of the fuzzy rules are based on the following situation.

(1) If $s(\dot{g}_x, t) < 0$ and $\dot{s}(\ddot{g}_x, t) < 0$, then decreasing k_j will increase $s(\dot{g}_x, t)\dot{s}(\ddot{g}_x, t)$ and the system will go towards the stable region.
(2) If $s(\dot{g}_x, t) > 0$ and $\dot{s}(\ddot{g}_x, t) > 0$, then increasing k_j will decrease $s(\dot{g}_x, t)\dot{s}(\ddot{g}_x, t)$ and the system will go towards the stable region.

The Fuzzy rule is formed by using discontinuous control law of Eq. (33)

$$u_{cx} = \begin{cases} 1 \text{ for } s(\dot{g}_x, t) > 0 \\ 0 \text{ for } s(\dot{g}_x, t) = 0 \\ -1 \text{ for } s(\dot{g}_x, t) < 0 \end{cases} \quad (33)$$

Based on the fuzzy rule described in Table 2, the FSMPWM can generate PWM signal for series converter, which provides series compensation voltage for compensating voltage sag/swell, voltage distortion, voltage unbalance and phase angle jump.

Simulation results and analysis

The proposed FSMPWM control technique of UPQC is modeled and simulated using MATLAB/SIMULINK. The UPQC model consists of a simple 50 Hz power distribution system with three- phase diode bridge rectifier feeding R_L, L_L load. The performance of UPQC with FSMPWM strategy is verified under different power quality conditions such as harmonics in supply current as well as voltage, load unbalance, voltage sag/swell, and supply voltage unbalance.

Table 3 shows the parameters used in the simulation, where R_{shf} and L_{shf} are the filter inductor for shunt active power filter, C_{dc} is the DC-link capacitor, V^*_{dc} is the DC-link reference voltage, L_{sef}, R_{sef} and C_{ef} are the inductance, resistance and capacitance of ac-filter circuit respectively for series converter and V_{rms} is the (RMS) value of the supply voltage.

The switching pulse generated using proposed FSMPWM control technique is shown in Fig. 10(a). From the figure it is observed that proposed control strategy provides constant switching frequency PWM signal, which minimizes the switching harmonics effects and enhances the tracking performance of UPQC. Subsequently, the tracking performances of source current and compensating voltage for conventional SMC as well as proposed FSMPWM control techniques are presented in Fig. 10(b). From the figure, it is clear that the proposed control strategy exhibits better tracking

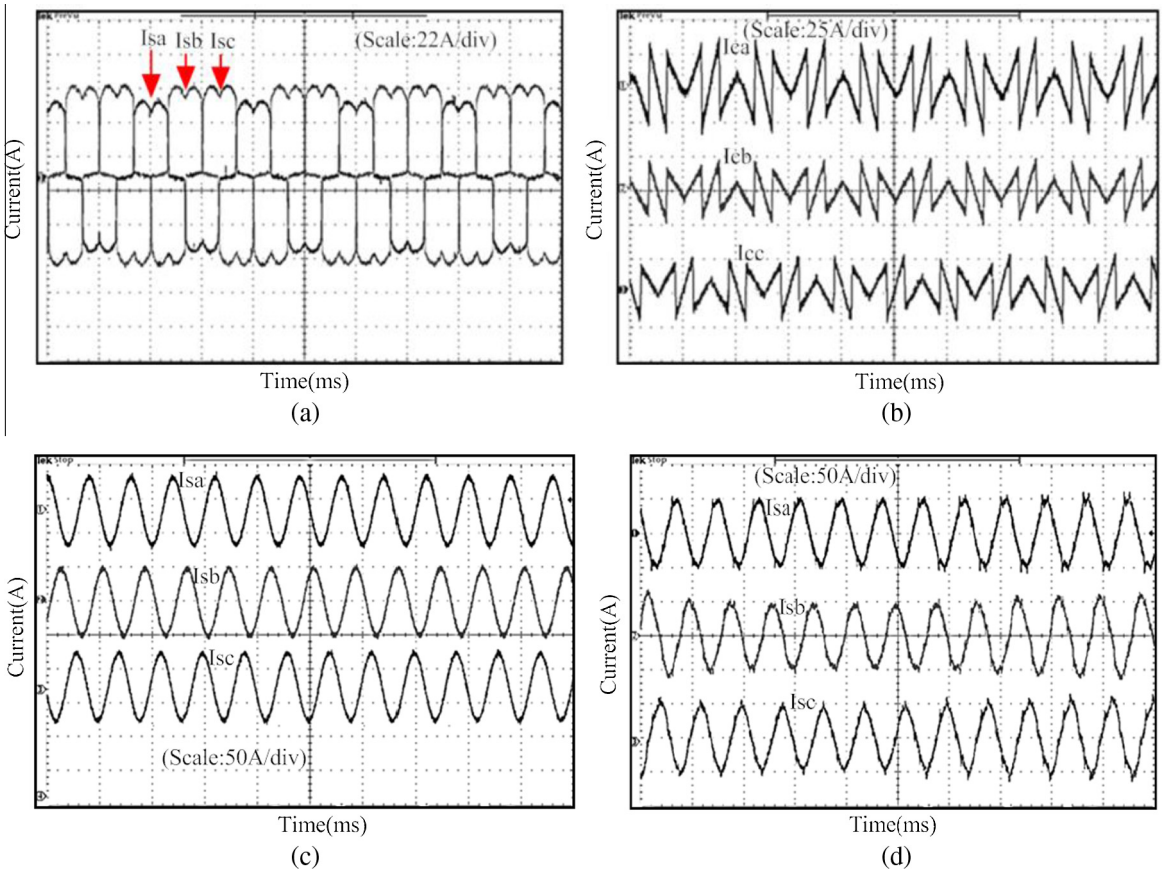

Fig. 19. Experimental results during load unbalanced condition, (a) source current before compensation under load unbalance condition, (b) compensation current under load unbalance condition, (c) source current after compensation under load unbalance condition using proposed method, and (d) source current after compensation under load unbalance condition using conventional SMC method.

performance irrespective of disturbance occurring in load side or source side. Therefore, it is observed from Figs. 11(a), (b) and 12 (b) that the current harmonics suppression capability of shunt converter in different load condition such as steady state, transient state and unbalance load condition is significantly improved in proposed FSMPWM control technique in comparison to conventional SMC technique [22]. Fig. 11(a) illustrates the waveforms of shunt converter during steady-state condition. From top to bottom the waveforms are source current before compensation, compensating current, source current after compensation using proposed method and source current after compensation using conventional SMC method respectively. From the results, it is clear that the proposed FSMPWM current control technique for shunt converter of UPQC provides an effective compensation of current harmonics reducing from 31.25% to 2.16% total harmonic distortion (THD) in the source current. However, conventional SMC controller exhibits some amount of distortion in source current as analyzed form figure. The primary causes behind these distortions are due to the chattering effect of conventional SMC during tracking the reference current. Thus, the source current THD is reduced up to 3.87%.

The performance of current harmonics filtering of shunt converter during load transient condition is illustrated in Fig. 11(b). During transient state the source current THD before compensation is found to be 33.42%, whereas, THD of source current after compensation is found to be 2.36% and 4.37% with the proposed and conventional SMC method, respectively. Thus, a margin level of 2.01% is noticed, which signifies that the proposed FSMPWM is capable of operating effectively for the wide range of power system operating condition.

Similarly, Fig. 12(a) highlights the performance of proposed FSMPWM controller during load unbalanced condition. From the figure it is observed that, proposed control strategy provides robust performance by restoring the source current in balanced condition and efficiently eliminates the harmonics from the source current in the wide range of load variation. Therefore, the source current THD before compensation is 30.61% and is reduced to 2.12%. However, conventional SMC method reduces the source current THD up to 3.36%. Table 4 summarizes the THD comparison of proposed FSMPWM technique and conventional SMC method during steady state, transient state and unbalanced load condition.

Fig. 12(b) demonstrates the performance of UPQC for voltage distortion compensation with both proposed and conventional SMC control method. The source voltage, compensating voltage, and load voltage after compensation with proposed method and load voltage after compensation with conventional SMC are shown in figure from top to bottom order respectively. Table 4 illustrates the THD comparison of source voltage during distortion condition and load voltage after compensation. From the tabulation, it is observed that THD of load voltage after compensation is around 1.52% in proposed method, whereas it is 2.86% in case of conventional SMC.

Fig. 13(a) analyzes the DC-link voltage performance of proposed controller during steady and transient state condition of load and supply voltage. The transient condition involves with sudden load change at 0.15 s, voltage sag/swell and load and source voltage unbalance. During these transient conditions voltage across the DC-link capacitor deviates from its reference value. The magnitude of the DC-link voltage deviation depends on the size of a load

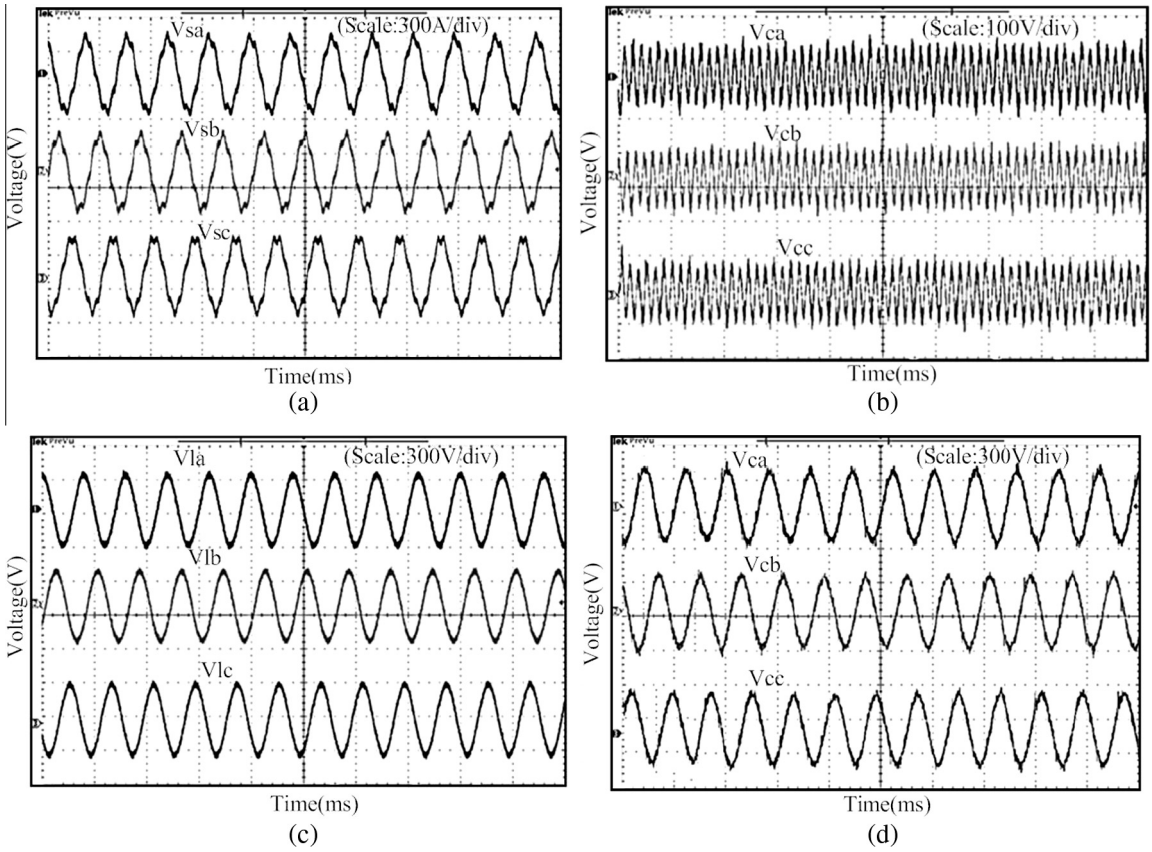

Fig. 20. Experimental results during voltage distortion conditions (a) source voltage, (b) compensation voltage, (c) load voltage after compensation using proposed method, and (d) load voltage after compensation using conventional SMC method.

connected, disconnected to the power distribution line and depth of sag/swell on the supply side. The DC-link voltage of proposed controller method for steady state load condition, transient load condition, unbalanced load condition, voltage sag/swell and supply voltage unbalance is shown in figure from top to bottom order. However, it is observed from the figure that the variations of DC-link voltage are quite satisfactory. The capacitor voltage is able to settle down within a minimum amount of time, both in initial and transient stage condition of load and supply voltage.

Further, in case of sag/swell conditions, we consider 30% of sag and 20% of swell, occurring in the interval of $0.12\ \text{s} \leqslant t \leqslant 0.21\ \text{s}$ for five cycles of ac-mains. Fig. 13(b) shows the compensation effect of proposed technique during the sag and swell condition respectively. From the top to bottom, the waveforms observed are supply voltage, compensating voltage, load voltage of both sag and swell condition. Fig. 14 illustrates the graphical representation of current and voltage harmonic spectrum of both the proposed method and conventional SMC method.

The efficacy of the proposed method during unbalanced supply voltage condition is depicted in Fig. 15(a). Figure shows the corresponding unbalanced supply voltage, compensating voltage, and load voltage after compensation from top to down order respectively. The series converter of UPQC detects the unbalanced voltage and injects unequal voltages so that the load voltage is regulated to its nominal value. The result of simulations for an occurrence of phase angle variation and phase angle jump during sag condition is shown in Fig. 15(b). The sag event has caused phase angle variation and jump during starting time of sag at $t = 0.12$ ms and clearing time of sag at $t = 0.21$ ms. As shown from the figure, the series converter of UPQC can inject appropriate compensation phase angle voltage for compensating the phase angle variation and jump in the supply voltages. Thus, the supply voltage is reinstated to its nominal voltage.

Experimental analysis using real-time HIL system

A real-time HIL system is constructed to validate an effectiveness of the proposed control strategy of UPQC. Fig. 16(a) shows the laboratory experimental setup using HIL system. The HIL simulation is a system that is utilized in a development and test of complex real-time embedded systems. The real-time HIL system consists of an OPAL-RT digital simulator (OP5600) with OP5142 Xilinx SPARTAN-3(3xc3s5000) FPGA processor as shown in Fig. 16(b). The OPAL-RT is a real-time simulation platform equipped with Intel Quad-core 2.40 GHz processor of type QNX and Read Hat Linux operating system. The OP5142 Reconfigurable FPGA-based I/O Controller enables the distributed execution of Hardware Description Language (HDL) capacities and high-speed, high-density digital I/O in real-time models. OP5142 is optimized for Hardware-in-the-Loop (HIL) simulation applications, and particularly intended for utilization with Opal-RT's full line of real-time simulators. Thus, the HIL simulation is more efficient for controlling the real-time system.

Performance of the UPQC on the real-time HIL system is evaluated for current and voltage harmonics, supply sag/swell condition, voltage unbalance condition and phase-angle variation and jump during sag condition. For the experimental validation, the same set of system parameters and load conditions as specified in simulation analysis are considered. The real time experimental verifications for shunt inverter of UPQC during balanced load condition are depicted in Fig. 17. The experimentation has been accomplished at switching frequency of 10 kHz. Fig. 17 (a) –(c)

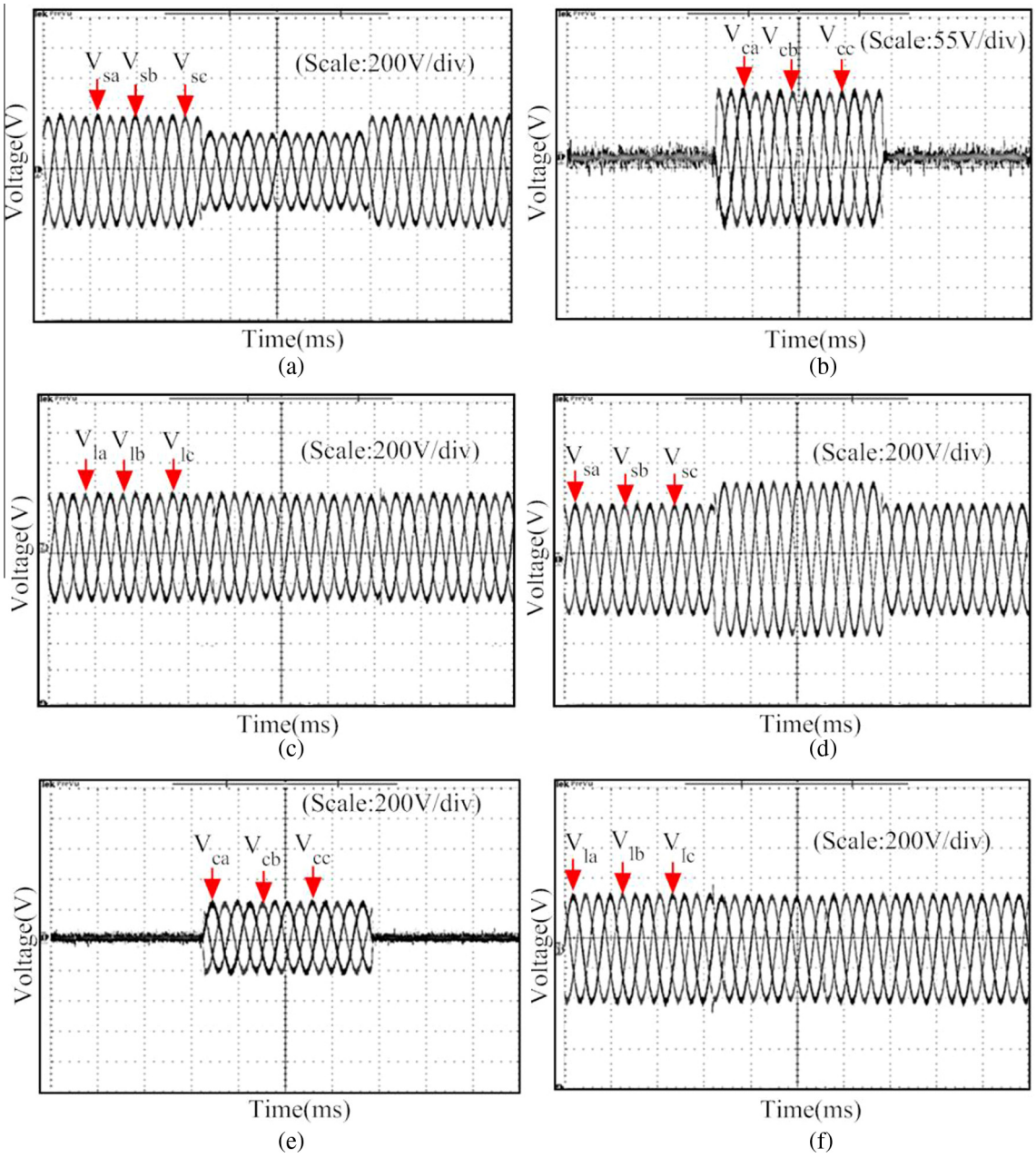

Fig. 21. Experimental results during sag/swell conditions, (a) sag voltage, (b) sag compensation voltage, (c) load voltage after compensation during sag condition, (d) swell voltage, (e) swell compensation voltage, and (f) load voltage after compensation during swell condition.

depict the steady-state performance of source current before compensation, compensating current and source current after compensation of proposed method respectively. Fig. 17(d) illustrates the source current after compensation of conventional SMC method. Fig. 18(a) shows the source current before compensation under transient state condition with a step change of load at $t = 0.15$ s. Fig. 18(b)–(d) provide the information about compensating current as well as source current after compensation with proposed method and conventional SMC method respectively. It is observed from figure that proposed controller effectively eliminates all harmonics from source current and makes the source current quite clean in nature without any ripples, whereas in conventional SMC method some ripples are found in the source current.

Fig. 19 demonstrates the compensation effect of shunt converter of UPQC for unbalanced load condition. The unbalance in the source current is created by connecting a resistive load (20 Ω) in series with phase *a* load resistance. This creates an unbalanced loading condition that can be observed from Fig. 19(a), therefore the phase *a* load current is reduced up to 48 A from its nominal value of 57 A. The shunt converter of UPQC generates the compensating current, which is observed from Fig. 19(b). From Fig. 19(b), it is clear that the amplitude of compensating current for phase *a* is raised up to 35 A as compared to phase *b* and phase *c*, where the amplitudes are 25 A. Fig. 19(c) and (d) shows the three-phase source current for the proposed and conventional SMC method respectively. This figure shows that the source current for the proposed method is more clean and balanced sinusoidal as compared to the conventional SMC method.

Fig. 20 shows the experimental result of distorted voltage compensation capability of the proposed algorithm. In this case, 1% of the 5th harmonic voltage has been mixed with the grid voltage to create distortion voltage. The series inverter of UPQC acts as a

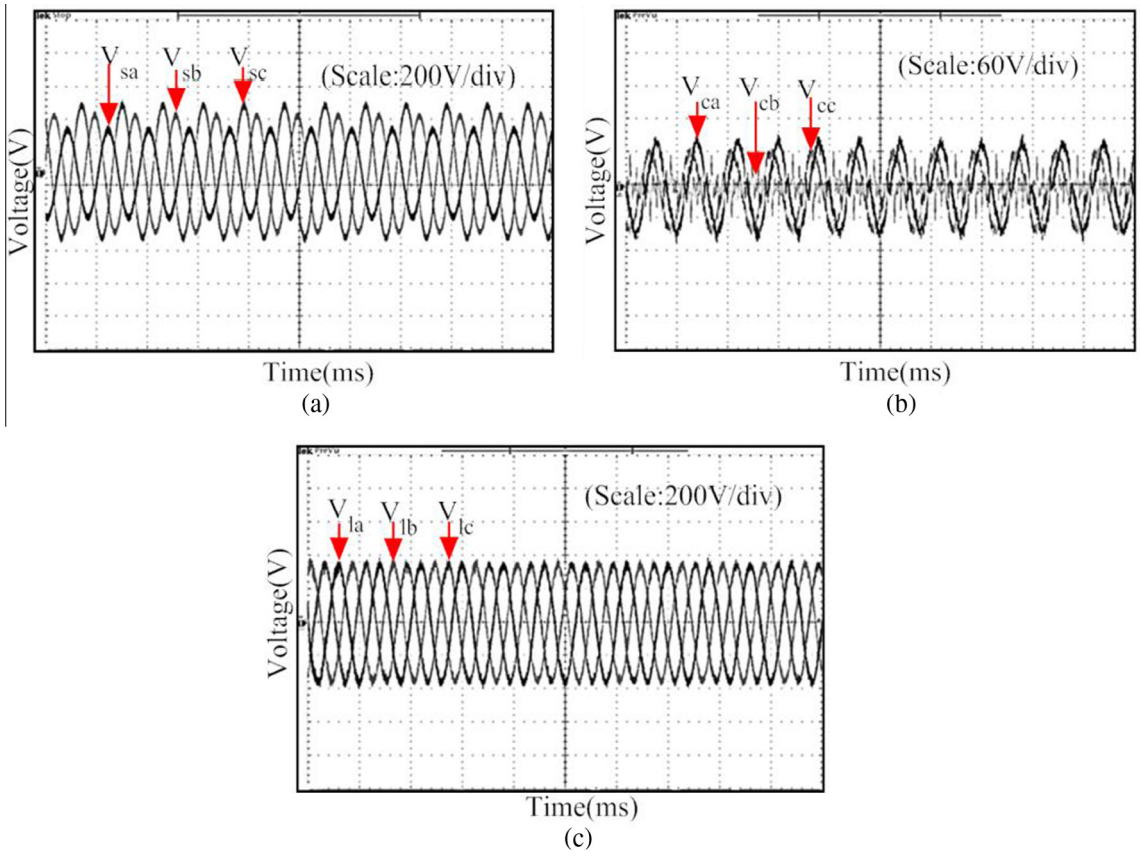

Fig. 22. Experimental results during unbalanced supply voltage condition using proposed method, (a) source voltage, (b) unbalance compensation voltage, and (c) load voltage after compensation.

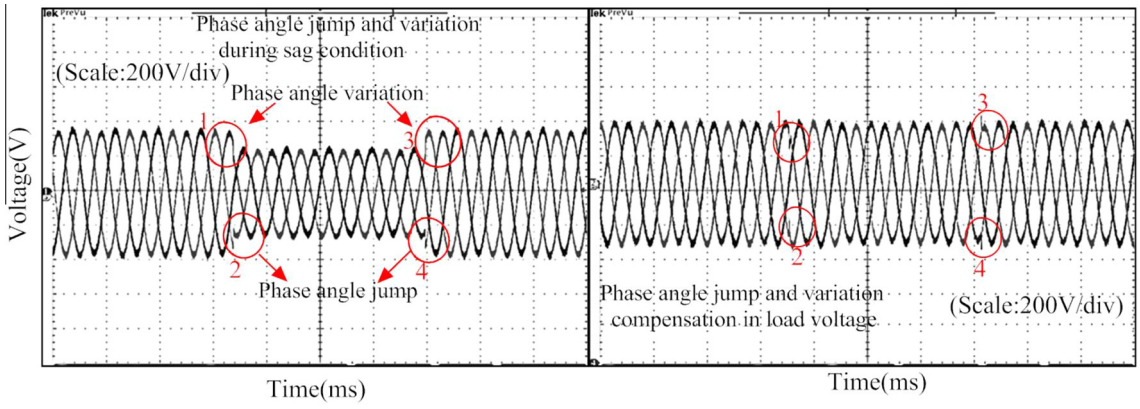

Fig. 23. Experimental results of phase-angle jump and variation compensation during sag condition.

series-type distortion voltage compensator to filter out all distortions present in the supply voltage and provides quality voltage to the load. Fig. 20(a)–(c) shows the experimental results of supply voltage under distortion condition, compensating voltage V_c and load voltage V_l respectively, whereas Fig. 20(d) shows the load voltage compensation capability of conventional SMC method. From the figure, it is observed that the load voltage waveforms V_{la}, V_{lb} and V_{lc} of proposed method are more sinusoidal in nature in comparison to the conventional method. Therefore, it is confirmed that by utilizing the proposed algorithm, series inverter of UPQC compensates the source voltage distortion effectively.

Fig. 21 shows the voltage sag/swell compensation capability of UPQC using proposed control technique. For examining the voltage sag compensation capability, 30% of voltage sag is considered for a period of five cycles. Fig. 21(a)–(c) shows the experimental results of supply voltage V_s, compensating voltage V_c and load voltage V_l respectively. The series inverter of the UPQC injects a proper voltage during voltage sag leading to a compensating load voltage. Fig. 21(d)–(f) represent experimental results of voltage swell compensation capability of the proposed algorithm. In this case, 20% of voltage swell for a time interval of five cycles has been applied to the grid.

Fig. 22 shows an experimental study of voltage unbalances compensation capability of the proposed algorithm. Fig. 22(a) shows the waveforms of the three phase unbalanced voltages. In this study, voltage unbalance is created by considering three different amplitudes such as $V_{sa} = 280$ V, $V_{sb} = 360$ V and $V_{sc} = 400$ V. Fig. 22(b) and (c) depict compensation voltage and load voltage respectively. Series inverter of the UPQC injects the proper amount of compensating voltage for regulating the load voltage to its nominal value. Fig. 23 shows the experimental results of Phase-angle jump and variation compensation during sag condition. From the figure it is observed that proposed control technique can effectively reduce the phase-angle variation and phase-angle jump and can make the load voltage purely sinusoidal.

Conclusion

In this paper, a novel fixed frequency FSMPWM based control strategy is presented for UPQC. The proposed control methodology is responsible for fast and accurate tracking of the reference signal along with providing fixed switching frequency during power system perturbations and also eliminates the inherent chattering drawback of sliding mode control. Moreover, this control approach is designed for the inner current and voltage control loop of UPQC, where fuzzy rules are described with two inputs and its singleton defuzzification is utilized in generating PWM signals for both shunt and series converter. From the results it is observed that the proposed control strategy generates fixed switching frequency and provides better tracking performance than CSMC strategy. It is also observed from simulation and experimental result that proposed control strategy provides quick dynamic response and less steady-state error. Therefore, it successfully compensates several PQ problems such as current harmonics, load unbalance, voltage sag/swell, voltage unbalance, voltage distortion and phase-angle jump existing in the power distribution network and makes UPQC robust in comparison to the conventional SMC method during power system perturbations.

References

[1] Li P, Li Y, Yin Z. Realization of UPQC H∞ coordinated control in Microgrid. Int J Electr Power Energy Syst 2015;65:443–52.
[2] Esfahani MT, Hosseinian SH, Vahidi B. A new optimal approach for improvement of active power filter using FPSO for enhancing power quality. Int J Electr Power Energy Syst 2015;69:188–99.
[3] Rahmani B, Li W, Liu G. An Advanced Universal Power Quality Conditioning System and MPPT method for grid integration of photovoltaic systems. Int J Electr Power Energy Syst 2015;69:76–84.
[4] Pal Y, Swarup A, Singh B. A comparative analysis of different magnetics supported three-phase four-wire unified power quality conditioners – a simulation study. Int J Electr Power Energy Syst 2013;47:436–47.
[5] Patjoshi RK, Mahapatr KK. Non-linear sliding mode control with SRF based method of UPQC for power quality enhancement. In: 9th International IEEE conference of industrial and information systems (ICIIS). p. 1–6.
[6] Kinhal VG, Agarwal P, Gupta HO. Performance investigation of neural-network-based unified power-quality conditioner. IEEE Trans Power Delivery 2011;26(1):431–7.
[7] Patjoshi RK, Mahapatra KK. Resistive optimization with enhanced PLL based nonlinear variable gain fuzzy hysteresis control strategy for unified power quality conditioner. Int J Electr Power Energy Syst 2016;83:352–63.
[8] Karanki SB, Mishra MK, Kumar B. Particle swarm optimization-based feedback controller for unified power-quality conditioner. IEEE Trans Power Delivery 2010;25(4):2814–24.
[9] Patjoshi RK, Mahapatra KK. New control strategy of unified power quality conditioner with sliding mode approach. Mumbai: IEEE INDICON; 2013. p. 1–6.
[10] Rahman SA, Janakiraman PA, Somasundaram P. Voltage sag and swell mitigation based on modulated carrier PWM. Int J Electr Power Energy Syst 2015;66:78–85.
[11] Khan JF, Bhuiyan SM, Rahman KM, Murphy GV. Space vector PWM for a two-phase VSI. Int J Electr Power Energy Syst 2013;51:265–77.
[12] Monfared M, Rastegar H. Design and experimental verification of a dead beat power control strategy for low cost three phase PWM converters. Int J Electr Power Energy Syst 2012;42(1):418–25.
[13] Monter AR, Bueno EJ, García-Cerrada A, Rodríguez FJ, Sánchez FM. Detailed analysis of the implementation of frequency-adaptive resonant and repetitive current controllers for grid-connected converters. Electric Power Syst Res 2014;116:231–42.
[14] Shieh CS. Fuzzy PWM based on Genetic Algorithm for battery charging. Appl Soft Comput 2014;21:607–16.
[15] Venkataramanan G, Divan D. Discrete time integral sliding mode control for discrete pulse modulated converters. In: Power Electron Specialists Conf. p. 67–73 [21st Annual IEEE].
[16] Abrishamifar A, Ahmad AA, Mohamadian M. Fixed switching frequency sliding mode control for single-phase unipolar inverters. IEEE Trans Power Electron 2012;27(5):2507–14.
[17] Fang Y, Fei J, Mab K. Model reference adaptive sliding mode control using RBF neural network for active power filter. Int J Electr Power Energy Syst 2015;73:249–58.
[18] Yan W, Hu J, Utkin V, Xu L. Sliding mode pulsewidth modulation. IEEE Trans Power Electron 2008;23(2):619–26.
[19] Morris S, Dash PK, Basu KP. A fuzzy variable structure controller for STATCOM. Electric Power Syst Res 2003;65(1):23–34.
[20] Yu FM, Chung HY, Chen SY. Fuzzy sliding mode controller design for uncertain time-delayed systems with nonlinear input. Fuzzy Sets Syst 2003;140(2):359–74.
[21] Yagiz N, Hacioglu Y, Taskin Y. Fuzzy sliding-mode control of active suspensions. IEEE Trans Ind Electron 2008;55(11):3883–90.
[22] Saetieo S, Devaraj R, Torrey DA. The design and implementation of a three-phase active power filter based on sliding mode control. IEEE Trans Ind Appl 1995;31(5):993–1000.
[23] Ucar M, Ozdemir S. 3-Phase 4-leg unified series–parallel active filter system with ultracapacitor energy storage for unbalanced voltage sag mitigation. Int J Electr Power Energy Syst 2013;49:149–59.
[24] Jeraldine Viji A, Aruldoss Albert Victoire T. Enhanced PLL based SRF control method for UPQC with fault protection under unbalanced load conditions. Int J Electr Power Energy Syst 2014;58:319–28.